Scientific Research Publishing

World Journal of Nano Science and Engineering, 2021, 11, 25-43
https://www.scirp.org/journal/wjnse
ISSN Online: 2161-4962
ISSN Print: 2161-4954

Er^{3+} and Er^{3+}/Yb^{3+} Ions Embedded in Nano-Structure $BaTi_{0.9}Sn_{0.1}O_3$: Structure, Morphology and Dielectric Properties

Olfat El Sayed[1], Inas Battisha[2*], Abdelilah Lahmar[3], Mimoun El Marssi[3]

[1]Physics Department, Faculty of Women for Arts, Science and Education, Ain Shams University, Cairo, Egypt
[2]Solid State Physics Department, Physics Research Division, National Research Centre, Dokki, Giza, Egypt
[3]Laboratory of Condensed Matter Physics (LPMC), University of Picardie Jules Verne, Amiens, France
Email: olfat.elsayed@women.asu.edu.eg, *ibattisha@gmail.com, abdel.ilah.lahmer@u-picardie.fr, mimoun.elmarssi@u-picardie.fr

How to cite this paper: El Sayed, O., Battisha, I., Lahmar, A. and El Marssi, M. (2021) Er^{3+} and Er^{3+}/Yb^{3+} Ions Embedded in Nano-Structure $BaTi_{0.9}Sn_{0.1}O_3$: Structure, Morphology and Dielectric Properties. *World Journal of Nano Science and Engineering*, **11**, 25-43.
https://doi.org/10.4236/wjnse.2021.112002

Received: May 23, 2021
Accepted: June 26, 2021
Published: June 29, 2021

Abstract

Barium titanate tin oxides $BaTi_{0.9}Sn_{0.1}O_3$ referred to as (BTSO) doped with $0.5Er^{3+}$ and co-doped with (0.75 and 1) Yb^{3+} ions, were prepared using a modified sol-gel method and calcinated at 1050˚C in the air for 4 h. The influence of the selected rare earth element on the structure morphology, dielectric properties behavior was investigated. From TEM micrographs, it has appeared that the particles have a spherical shape with a small size in nanoscale. The average particle size is determined both by TEM and XRD diffraction was found to be in agreement and within the range between 45.9 and 57.7 nm. The effects of Lanthanide incorporation on the evolution of these nano-crystalline structures were followed by XRD and (FTIR). The XRD patterns give rise to a single perovskite phase, while the tetragonality was found to decrease gradually with Er^{3+} and Er^{3+}/Yb^{3+} ions, respectively. FTIR results showed enhancement of the crystallinity and the absence of carbonates upon increasing Yb^{3+} ions concentration from 0.75 up to 1 mol%. The dielectric and conductivity properties were found to be enhanced by the nature and the concentration of the lanthanide element (Er^{3+}, Yb^{3+}) in the BTSO host lattice. The Curie temperature (T_c) shifted to a lower value from 117 for BTSO: 0.5Er to 93 for BTSO: 0.5Er/1Yb and the permittivity ε' increased from 3972 to 6071, so BTSO: 0.5Er/1Yb good crystalline material candidate for capacitors application due to its higher permittivity.

Keywords

Sol-Gel, Nano-Structure $BaTiSnO_3$-Doped, "Er^{3+} Ion" or "Er^{3+}/Yb^{3+} Ion", Dielectric Properties

1. Introduction

Barium titanate material $BaTiO_3$ (BTO) is the most known perovskite that attracts, and still does, particular interest due to its high dielectric constant and low ferroelectric phase transition temperature compatible with a large number of industrial applications. Especially in the electronics industry for ultrasonic devices, ferroelectric memories, dielectric capacitors, resistors, as well as in filters [1] [2]. The materials having ABO_3 perovskite structure were obtained wider attraction because of their dielectric, ferroelectric, pyroelectric, and piezoelectric properties [3]. The ferroelectric materials having relaxor behavior exhibit a high-frequency dispersion of dielectric permittivity [4]. BTO is a class of ABO_3 perovskite structure, BTO with tetragonal perovskite structure is a good ferroelectric material which has been used in different applications such as microwave filters, mobile-communication technology resonators, and plays a major role in microwave devices [5].

The literature survey showed that different type of substituents has been reported either in Ba- or Ti-sites to improve BTO properties to satisfy the need and requirement of new devices technology. Among these elements, we found that the incorporation of rare earth (RE^{+3}) ions can change the dielectric/ferroelectric behaviors of BT and give rise to promising properties such as excellent electro caloric and energy storage properties [6] [7]. Recall that BTO endorses three types of phase transitions: Rhombohedral → Orthorhombic → Tetragonal → Cubic phase. The ferroelectric (tetragonal) to paraelectric (cubic) phase transition occurs at 120˚C and the orthorhombic to tetragonal transition occurs at very low temperature (~5˚C). Previous studies suggested that the adjusting of the ferroelectric phase transition temperature is possible by replacing partially titanium (Ti) with tin (Sn) [8] [9]. Further, it is shown that the introduction of Sn in the BT matrix improves the dielectric and resistivity behaviors. Owing to these possibilities, $BaTi_{(1-x)}Sn_xO_3$ (BTS) system attracts particular attention for applications [10].

It should be mentioned that several researches works reported the presence of a diffused phase transition in $Ba(Ti_{1-x}Sn_x)O_3$, for x~0.30 with the apparition of the relaxor characteristics [11]. Furthermore, an increase in permittivity, tunability under the biasing field, and a reduction of the low-frequency dielectric losses were also observed.

In the present work, the emphasis is placed on the oscillator behavior of RE^{3+} cations when it is incorporated into the BTSO matrix, noting that the lanthanide ions (Ln^{3+}) from Sm^{3+} to Er^{3+} have their intermediate size between Ba^{2+} and Ti^{4+} and they can be accommodated at any of both lattice sites (A or B), depending on stoichiometry and their doping concentration [11]. Interestingly, Erbium (Er^{3+}) has been widely used due to its promising technological interest, especially in telecommunication applications [12]. However, this element is known for its amphoteric behavior in the perovskite matrix [13] [14]. When it is in the B-sites, the electrical and luminescence properties are improved widely. In contrast, when it is located in the A-sites, the mentioned properties are deteriorating [13]. Thus,

understanding the behavior of this element in a selected perovskite matrix, alone and with other doping elements, as well as to shed light on the parameters that could influence such behavior are of most interest before any eventual application.

In this research, the present study aims to investigate the Er^{3+} ions presence influence (as well as the co-presence of Er^{3+}/Yb^{3+} ions) on the structural, morphology and dielectric properties of $BaTi_{0.9}Sn_{0.1}O_3$ (BTSO), prepared by the modified sol-gel method. The concentration effect of the lanthanide element is also highlighted in this work using different techniques of characterizations such as microstructural, vibrational and electrical properties. We hope that this work will constitute a helpful contribution to understanding the behavior of Yb^{3+} ions in a perovskite matrix.

2. Experimental Methods

2.1. Sample Preparation

Nano-structure BTSO doped with 0.5 mol% of Er^{3+} ions and co-doped with two different concentrations of Yb^{3+} ions 0.75 and 1 mol%, refereed as (BTSO: 0.5Er) and (BTSO: 0.5Er0.7Yb and 1 BTSO: 0.5Er1Yb), respectively were prepared with sol-gel method. The chemical reagents used in the present work were barium acetate $Ba(CH_3COO)_2$ (Aldrich 99%), titanium (IV) n-butoxide $Ti(OC_4H_9)_4$ (Alfa Aesar 99+%). Acetyl acetone $C_5H_8O_2$ (Aldrich 99+%) and acetic acid ($C_2H_4O_2$) diluted with distilled water (HAc)-H_2O were selected as solvents of titanium (IV) n-butoxide and barium acetate, respectively.

Firstly, Acetic acid ($C_2H_4O_2$) diluted with distilled water (HAc)-H_2O and acetyl acetone ($C_5H_8O_2$) were selected as solvents of $Ba(CH_3COO)_2$ and $Ti(OC_4H_9)_4$ respectively. BTO_3 obtained after the reacting of the following two solutions the former is for barium acetate and the last for titanium (IV) n-butoxide by stirring for suitable time (~1 h), the gel was formed at ~130˚C. Solution of $SnCl_4{\cdot}5H_2O$ dissolved in16 ml isopropanol (C_3H_8O) and stirred for 15 min referred as (tin solution). In the next step, Tin solution was added to titanate solution and stirred for another 15 min referred as (BTSO solution), by drying BTSO at 350˚C and annealed it at 1050˚C for 4 h in air, we can get BTSO ceramic material (host material). For preparing BTSO doped with 0.5 mol% of Er^{3+} ions a solution of 0.5 mol% of Er $(NO_3)_3{\cdot}6H_2O$ dissolved in 5 ml of (HAc)-H_2O was added to the BTSO solution and stirred for 45 min, dried at 350˚C and annealed to obtained BTSO: 0.5Er compound. Similar procedure was used for Er^{3+} and Yb^{3+} Co-doped samples, but with the addition of $Yb(NO_3)_3{\cdot}5H_2O$ dissolved in 5ml of distilled water. The Gel formed at ~130˚C was dried, and then the densification was done by calcination in air at 1050˚C for 4 h using Muffle furnace (type Carbolite CWF 1200). Nano-structure powder samples were produced.

2.2. Characterization

2.2.1. Structural and Vibrational Analysis

X-ray Diffraction (XRD) measurements for all prepared polycrystalline samples

were performed at room temperature using the X-ray diffractometer with Cu $K_{\alpha 1}$ radiation. The Crystallite Size (C.S.) was calculated by the Scherer's equation [15]:

$$\text{C.S.} = K\lambda / B\cos\theta \tag{1}$$

where λ = 1.5406 Å is the wavelength, K = 0.89 is Scherer constant, the full width at half maximum (FWHM) intensity of the peak (in radians) is B and the diffracted angle is θ.

The chemical structure and function groups of all specimens were measured at room temperature by FTIR spectroscopy (thermo Nicolet, FTIR and NEXUS) in the range from 4000 - 400 cm^{-1} using the potassium bromide (KBr) disc technique. The samples powders were mixed with KBr and preparing the discs, the IR absorption spectra were measured immediately.

The internal structure of the prepared samples was observed using a Transmission Electron Microscope (TEM; JEOL JEM-1230) its magnification power reaches to 600 kx and resolving power down to 0.2 nm. And also accelerating voltage 100 kV, can reach to 120 kV with attached CCD camera through steps. The samples were prepared before observation by making a suspension solution using ultrasonic water bath from dissolving powder in distilled H_2O. Take a drop of the suspension and then put into a grid of carbon and left it to dry. In TEM, the sample is exposed to highly accelerated electrons beam. When the electrons are passing through the sample, they interact with the material. Field emission scanning electron microscope FESEM instrument provided with variable pressure (FEI, model: Quanta 250 FEG).

2.2.2. Dielectric Measurements

For dielectric measurements, the fine ceramic powders were pressed into samples-shaped pellets having diameter of 13.09 mm and thickness of 2 mm under pressure of 40 MPa at room temperature. To ensure good contacting, both surfaces of each sample were coated with silver paste, then inserted between two conducting parallel plates (forming capacitor plates) The dielectric measurements were carried out by inserting the ($BaTiSnO_3$ doped with Er^{3+} and co-doped with Er^{3+}/Yb^{3+} ions) samples between two conducting parallel plates forming capacitor. Sample temperature was controlled by thermometer contact to the sample and temperature controller. IM3570 which serves as both an LCR meter and an Impedance Analyzer, was used to measure the dielectric properties over a wide frequency range (10^1 - 10^5 Hz) and temperature range (−100˚C to 200˚C). The dielectric properties namely; the permittivity (ε'), dielectric loss (ε'') and AC conductivity (σ_{ac}) were calculated as follows:

$$\varepsilon' = \frac{Cd}{\varepsilon_o A} \tag{2}$$

$$\varepsilon'' = \varepsilon' \tan\delta \tag{3}$$

$$\sigma_{ac} = \omega\varepsilon_o\varepsilon'' \tag{4}$$

where C is the electrical capacitance in Farad, ε_o is the permittivity of free space

(8.854×10^{-12} F/m), $\tan\delta$ is the loss tangent, d is the sample thickness and A is the sample surface area.

3. Results and Discussion

3.1. X-Ray Diffraction

Figure 1 shows the XRD patterns of BTSO: 0.5Er (A), BTSO: 0.5Er0.75Yb (B) and BTSO: 0.5Er1Yb (C) powders calcinated at 1050˚C for 4h in air. XRD reflections are completely matched and indexed using ICDD card N˚ [74-2491] with tetragonal perovskite symmetry for BTO pure powder. As previously reported for pure BTO and BTSO, d spacing (lattice parameters) increases as a result of substitution of Ti^{4+} with larger ionic radius of Sn^{4+} and/or (RE^{3+}) Rare earth elements [16] [17] [18]. By focusing on the peak at theta equal to 31˚ it is appeared that Er^{3+} and Yb^{3+} doping causes no shift in the peak position. From our previous work, it is clearly indicated that Sn^{4+} is systematically dissolved in BTO lattice with residuals of SnO_2 [19]. In the present work (Figure 1) represent BTSO doped samples (A, B, and C), from Figure 1, it is clearly observed that SnO_2 traces still present with various intensities. Also the intensities of the peaks in the spectrum B and C increases by increasing the concentration of Yb^{3+} ions without shift appeared in the peak positions and also without any observable phase change. Furthermore, the principle sharp peak appeared at $2\theta = 31.51^{\circ}$ dictated the tetragonal phase presence [20], without secondary phase appearance referring to Er^{3+} and/or Yb^{3+} ions, in the limit of device detection, so these ions suggested to be completely embedded in the BTSO crystal lattice. All the obtained values are gathered with the calculated lattice parameters in Table 1. The effect of Yb^{3+} ions concentration on the structure of BTSO: 0.5Er could be spotted from the Table 1. So, the lattice parameter (c) decreases while the lattice parameter (a) increases as the Yb^{3+} ions concentration increase, causing a decrease in the tetragonality ratio (c/a values). From Table 1, it is also seen that the crystallite size of BTSO: 0.5Er equal to 45.9 nm which, increases to 47.20 and then to 57.7 nm by increasing the co-doped concentration from 0.75 up to 1 mol% Yb, respectively this may be due to the substitution of Ti^{4+} ions by Er^{3+} and Yb^{3+} ions, where, they have larger ionic radius than Ti^{4+} ions. The powder diffraction patterns contain definite sharp peaks, representing good crystallinity for the samples. However, small shifts in the peak positions were resulted when the Yb^{3+} cations were embedded into the host BTSO: 0.5Er matrix.

Table 1. Chemical formula, calculated lattice parameters, tetragonal factor (c/a), crystallite size and Structure of nano-structure BTSO: 0.5Er, BTSO: 0.5Er0.75Yb and BTSO: 0.5Er1Yb samples calcinated at 1050˚C for 4 hours in the air.

RE^{3+} Concentrations %	Chemical formula	Lattice parameters		Tetragonal factor (c/a)	C.S from XRD (nm)	Structure
		a, b (Å)	c (Å)			
BTSO: 0.5Er	$BaTi_{0.85}\ Sn_{0.1}\ Er_{0.05}\ O_3$	3.9942	4.0120	1.0044	45.9	Tetragonal
BTSO: 0.5Er0.75Yb	$BaTi_{0.8425}\ Sn_{0.1}\ Er_{0.05}\ Yb_{0.0075}O_3$	4.0047	4.0192	1.0036	47.20	Tetragonal
BTSO: 0.5Er1Yb	$BaTi_{0.84}\ Sn_{0.1}\ Er_{0.05}\ Yb_{0.01}O_3$	4.0057	4.0160	1.0025	57.70	Tetragonal

The ionic radii of Ba^{2+}, Ti^{4+}, Er^{3+} and Yb^{3+} are ~1.61, ~0.605, ~0.89 and ~0.86 Å, respectively, the RE^{3+} ions site occupancy in ABO_3 material is well explained based on the thermodynamic considerations and tolerance factor through Tsur *et al.* [21] [22]. According to the study of Zulueta *et al.* [22] and Tsur *et al.*, Er^{3+} ions can found in both A-sites and B-sites (*i.e.* amphoteric effect), but basing on other previous studies Er^{3+} and Yb^{3+} ions would occupy B-site to improve the stability of BTO at this location [23] [24] [25] [26]. In the present work we study the substitution of RE^{3+} ions of Er^{3+} and Yb^{3+} in Ti-site (B-site) of BTSO nano-structure perovskite, the used concentration chemical formula are listed in **Table 1**. The XRD data are completely matched with the ICDD card no [74-2491] of tetragonal for all samples. As shown in **Figure 1**. appearance of un-desirable minority phases of SnO_2 their percent increased by increasing co-doping concentration of Yb^{3+} ions from 0.75 up to 1 mol%. And the absence of secondary phase referring to Er^{3+} confirms its substitution in Ti-site [24].

3.2. FTIR Analysis

FTIR spectra of all investigate samples are shown in **Figure 2** and all observed vibration modes are collected in **Table 2**. Noting that the absorption broad band at 561 cm^{-1} in the spectrum of BTSO: 0.5Eris assigned to M-O stretching vibration along the polar axis of spontaneous polarization. This mode which is the characteristic of the Ti-O and or Sn-O (M-O) vibration modes, becomes clearer [27]. This band shifted to 553 and 584 cm^{-1} in the spectrum of BTSO: 0.5Er0.75Yb and BTSO: 0.5Er1Yb respectively. The difference appeared in band positions could be caused by different lengths, strengths, and effective mass of the metal oxygen bonds formed by Sn, Er, Yb in B sites of the tetragonal $BaTiO_3$ structure [28]. The weak bands at 854 and 1031 cm^{-1} are assigned the vibration of carbonate group (CO_3^{2-}). We observed that this second band shifted to 1041 and 1043 cm^{-1} for BTSO: 0.5Er0.75Yb and BTSO: 0.5Er1Yb respectively [29]. However, the weak band at 1388 cm^{-1} is assigned to lattice carbonate attributed to CO_3^{2-}

Table 2. Band positions (cm^{-1}) and assignment of Infrared spectra of investigated various nano-structure BTSO: 0.5Er, BTSO: 0.5Er0.75Yb and BTSO: 0.Er1Yb calcinated at 1050˚C for 4 h in the air.

Wavenumber [cm^{-1}] BTSO: 0.5Er	Wavenumber [cm^{-1}] BTSO: 0.5Er0.75Yb0	Wavenumber [cm^{-1}] BTSO: 0.5Er1Yb	Relative intensity	Band assignments
561	553	584	Broad	M-O stretching vibration
854	852	852	Weak	CO_3^{2-} bending vibration
1031	1041	1043	Weak	CO_3^{2-} bending vibration
1388	1380	1386	Weak	CO_3^{2-} stretching vibration
1434	1434	1434	Weak	CO_3^{2-} stretching vibration
1629	1629	1629	Medium	O-H bending vibration
2856	2857	2857	Weak	C-H stretching vibrations (CH_2 group)
2923	2925	2925	Medium	C-H stretching vibrations (CH_3 group)
3442	3432	3438	Very broad	O-H stretching vibration

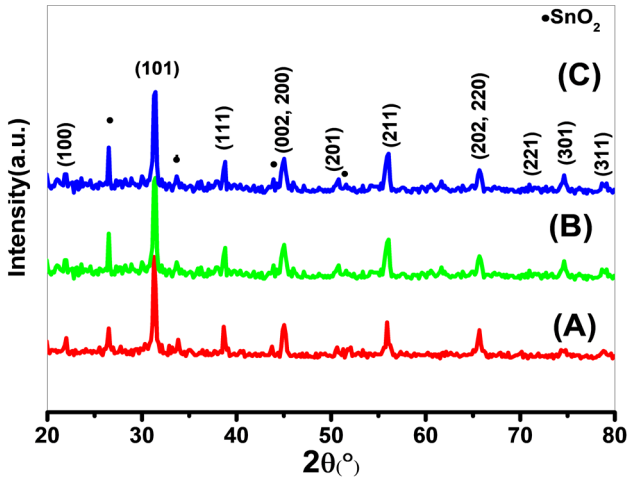

Figure 1. The XRD patterns of BTSO: 0.5Er (A), BTSO: 0.5Er0.75Yb (B) and BTSO: 0.5Er1Yb (C) nano-structure powders calcinated at 1050˚C for 4 hours in the air.

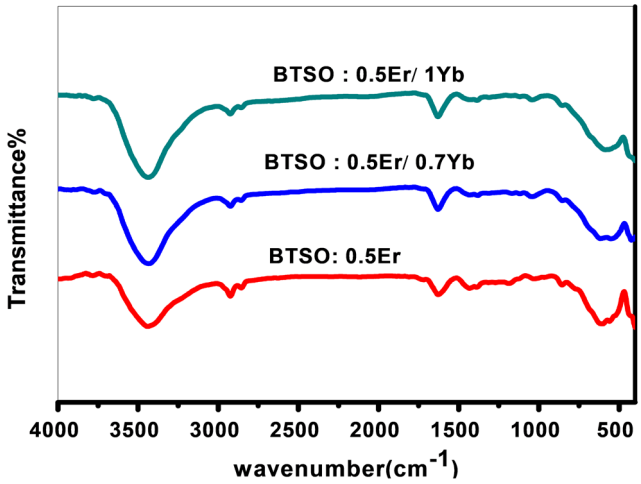

Figure 2. FTIR spectra of nano-structure BTSO: 0.5Er, BTSO: 0.5Er0.75Yb and BTSO: 0.5Er1Yb calcinated at 1050˚C for 4 hours in the air.

bending vibration. It is decreased in intensity by increasing the concentration of Yb^{3+} ions. Also, the weak band at 1434 could be assigned to the CO_3^{2-} stretching vibration [30]. Concerning the medium band observed at 1629 cm^{-1} in all the spectra, it is due to the decomposition mode of the absorbed H_2O molecules which is attributed to O-H bending vibration [31]. For the two very weak bands at 2856 and 2923 cm^{-1} observed in the spectrum of BTSO: 0.5Er, are assigned to C-H stretching vibrations for CH_2 and CH_3 respectively. They have small obvious intensity for doped Er^{+3} ions which decrease by increasing the concentration of co-doped Er^{+3}/Yb^{3+} ions, while the Very broad band at 3442 cm^{-1} in the spectrum of BTSO: 0.5Er are assigned to O-H stretching vibration modes of surface adsorbed water and shifted at 3432 cm^{-1} in the spectrum of BTSO: 0.5Er0.75Yb [32]. As conclusion, we can detect a little bit change between the spectra of both BTSO: 0.5Er0.75Yb and BTSO: 0.5Er1Yb due to the small difference in Yb^{3+} ions

content (0.3 mol%).

3.3. Transmission Electron Microscope (TEM) Analysis

The BTSO: 0.5Er morphology properties as example powder can be described based on the microstructure, as appeared in Figure 3(A) and Figure 3(B). TEM image of BTSO: 0.5Er powders calcinated in air for 4 h at 1050˚C is illustrated in

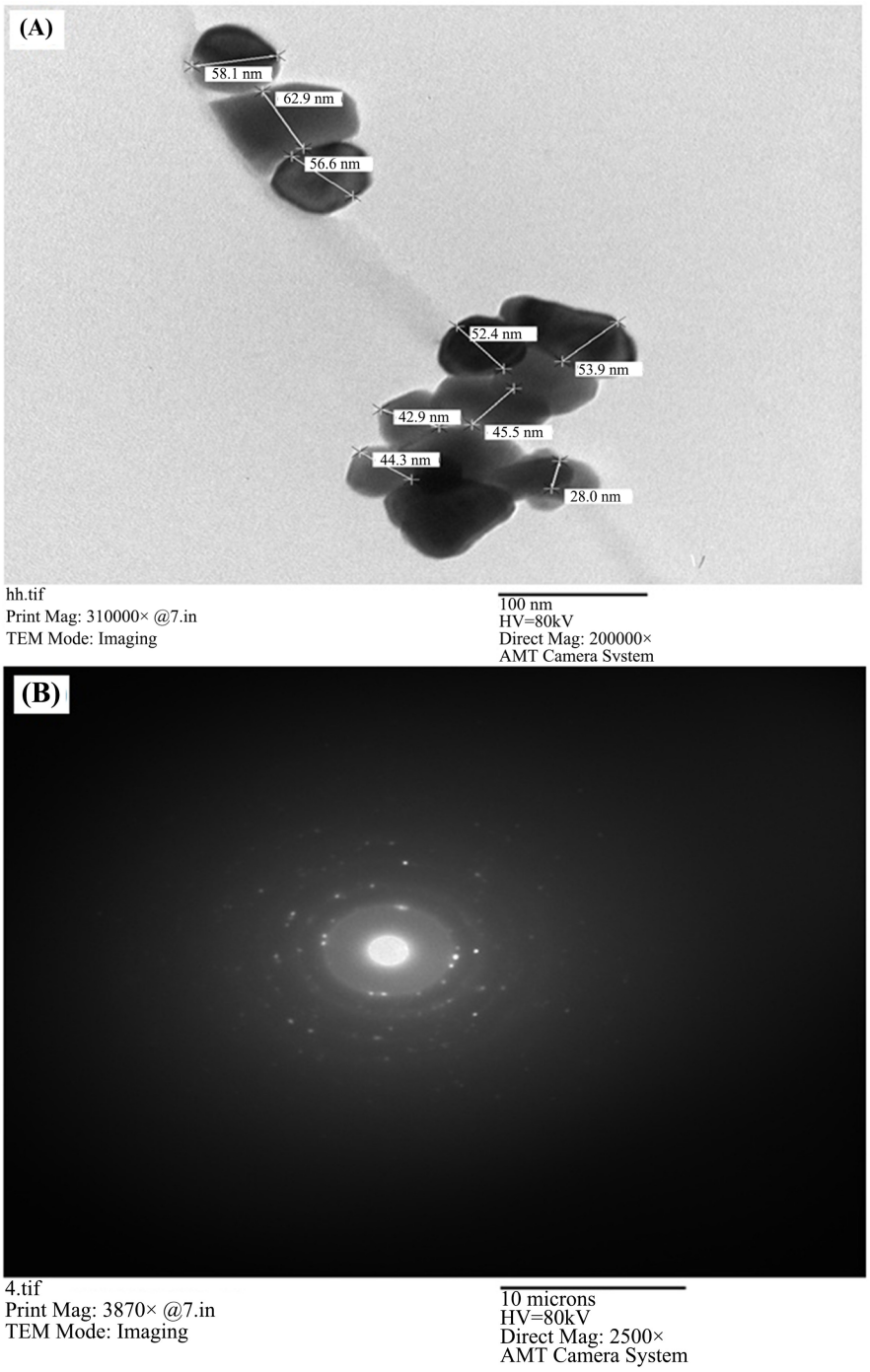

Figure 3. TEM micrographs (A) and the electron diffraction pattern (B) of BTSO: 0.5Er calcinated in air for 4 h at 1050˚C.

Figure 3(A). It is clearly seen some agglomerate clusters containing many small grains with tetragonal shape that could be a signature of crystallinity properties of samples [33]. The particle size was obtained by averaging the crystallite size total number in the TEM (JEOL JEM-1230) micrograph. On the basis of this method, BTSO: 0.5Er powder average crystallite size was 49.4 nm, which in good agreement with results obtained for crystallite sizes in the XRD study, possibly resulting from the fact that the identical strain within the particles that would induce the line broadening in XRD pattern were unfilled into account [34]. Further, the pattern of electron diffraction selected-area (SAED) obtained from the same sample TEM appeared in Figure 3(B). The (SAED) pattern indicates that the examined sample is assigned to perovskite nano-structure tetragonal phase [35].

3.4. FESEM Characterization

The morphology of the samples BTSO: 0.5Er, BTSO: 0.5Er0.75Yb and BTSO: 0.5Er1Yb ceramics calcinated in air for 4 h at 1050˚C were examined by the Field Emission Scanning Electron Microscopy (FESEM) are shown in Figures 4(A)-(C) respectively. Figure 4(A) shows the FESEM photographs associate to the surfaces of the BTSO: 0.5Er specimen with smaller grain sizes. Furthermore, some larger grains sizes are clearly observed from Figure 4(B) and Figure 4(C), the

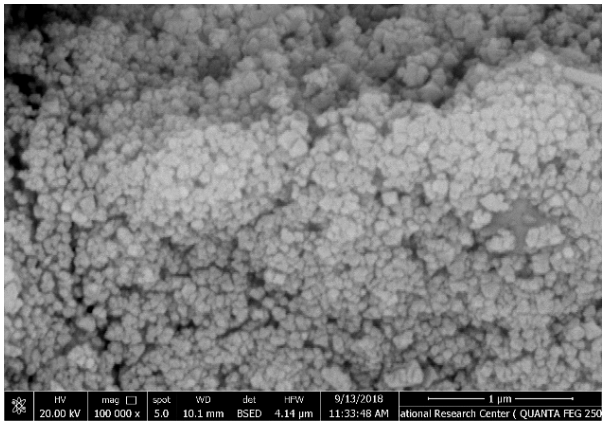

(A)

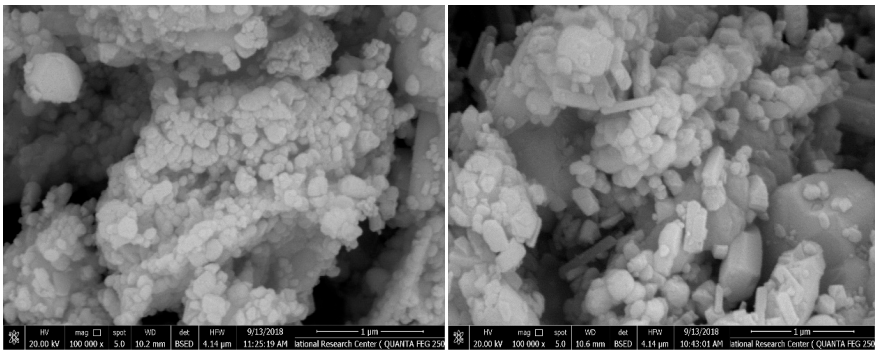

(B) (C)

Figure 4. FESEM micrograph of nano-structure BTSO: 0.5Er (A), BTSO: 0.5Er0.75Yb (B) BTSO: 0.5Er1Yb (C) calcinated at 1050˚C for 4 h in air.

significant grains size increases in the diameter, which is may be attributed to the doping with Er^{3+} and Yb^{3+} ion with larger ionic radius [36]. The average grain size of the samples BTSO: 0.5Er, BTSO: 0.5Er 0.75Yb and BTSO: 0.5Er1Yb were determined by linear intercept method from the surface of FESEM micrographs. The grain sizes are observed in the range between 31 and 52 nm. The grains become more obvious with higher density by increasing concentrations.

3.5. Dielectric Studies

3.5.1. The Temperature Dependence of the Permittivity (ε'), at Different Frequencies

The dielectric study of the BTSO: 0.5Er (A), BTSO: 0.5Er0.75Yb (B) BTSO: 0.5Er1Yb (C) calcinated at 1050˚C for 4 h in air permittivities (ε'), at different frequencies are studied for the first time **Figure 5**. To highlight on the effect of doping BTSO with 0.5 mol% of Er^{3+} ions and $0.5Er^{3+}/(0.7, 1)$ mol% of Yb^{3+}, the temperature dependence of the permittivity (ε') in the range between −100˚C to 200˚C at different frequencies (10^2 to 10^6 Hz) for the samples BTSO: 0.5Er and BTSO: 0.5Er/1Yb calcinated in air for 4 h at 1050˚C. The ionic radii for Er^{3+} and Yb^{3+} are ~0.89 and ~0.86 Å, respectively, but for Ba^{2+}, Ti^{4+} ions are ~1.61, ~0.605 Å, respectively. Therefore, ε'variation for these samples showed that the partial substitution of Ti^{4+} with Er^{3+} and/or Er^{3+}/Yb^{3+} ions have a prominent influence on the dielectric properties. The two samples exhibited round shape without sharp peak and the dielectric anomalies that correspond to three structural transitions [rhombohedral to orthorhombic ($T_{R\text{-}O}$), orthorhombic to tetragonal ($T_{O\text{-}T}$) and tetragonal to cubic ($T_{T\text{-}C}$)] could be detected for both BTSO: 0.5Er and BTSO: 0.5Er/1Yb. Having in mind that the temperature at which the structure transforms from tetragonal to cubic phase ($T_{T\text{-}C}$) is well known as Curie temperature (T_c) at which the unit cell undergoes a phase transition from the polarized state (tetragonal) to the un polarized state (cubic) or from the ferroelectric ionic radii to the para-electric [37]. Upon co-doping with Er^{3+}/Yb^{3+} ions, the shape of

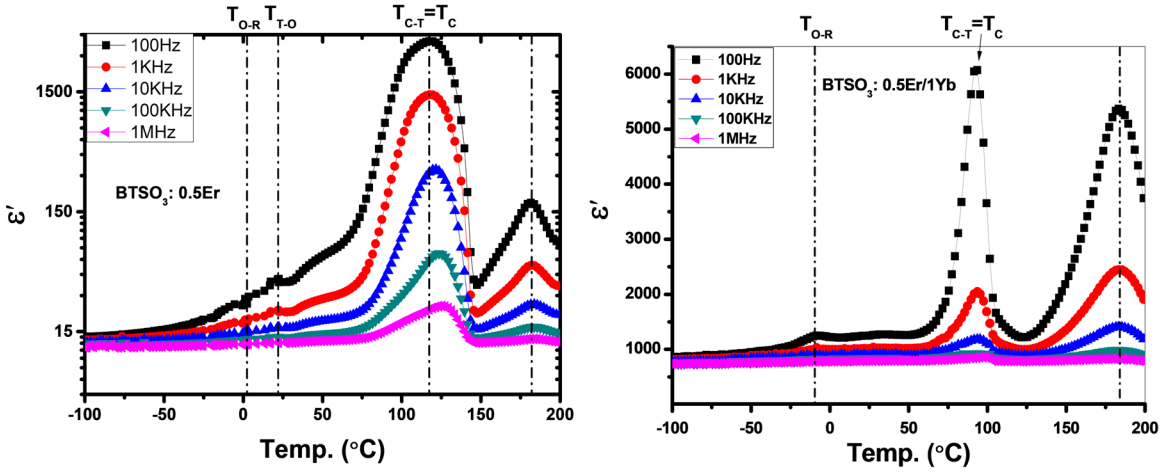

Figure 5. The temperature dependence of the permittivity (ε') at different frequencies for BTSO: 0.5Er and BTSO: 0.5Er/1Yb calcinated in air for 4 h at 1050˚C.

curves changed and the phase transitions temperature shifted to lower values. It is clearly seen that the T_c shifted from 117˚C for BTSO: 0.5Er to 93˚C BTSO: 0.5Er1Yb, respectively, which is in good accordance to tetragonality ratio calculated from XRD and also to the previously reported in literature [38]. Where Yb^{3+} ions with larger ionic radius than Ti^{4+} led the deformation of BTSO: 0.5Er perovskite structure and a reduction in its tetragonality, thus inducing a drop in the Curie temperature, and more drop induced with increasing Yb^{3+} ions doping concentration. From our previously report about BTSO its permittivity is equal to 2520 [19], comparing this result; the permittivity increased for BTSO: 0.5Er and BTSO: 0.5Er1Yb, it was found to be equal to 3972 and 6071, respectively at both the T_C temperature and the constant frequency measured at 10^2 Hz. The increase in the permittivity can be due to the modifications in the crystallite size as seen in **Table 1**, resulting from Er^{3+} and Er^{3+}/Yb^{3+} ions doping in the BTSO structure. These results confirmed that the known results for rare earth oxides: as they are function materials and can improve the dielectric properties of BT-based ceramics [16].

To detect the effect of adding the sensitizer Yb^{3+} ions, the mentioned increase in ε' by co-doping with the Yb^{3+} ions content has detected and attributed to the increase of Yb^{3+} ions concentration, where its absence may inhibit grain growth so reduction of grain size has occurred. On the other hand, such increase in ε' is related to the fact that Er^{3+} and Yb^{3+} ions have different lattice constants which add different stress in to the lattice as shown in the preceding, **Table 1** [39] [40]. The permittivity has an unexpected relaxation peak whose maximum (~181.5 and 183˚C) is positioned at temperature higher than T_c for both prepared samples. The reason for this hasn't been explained before, and then it will be an open point for future discussion. One may explain this relaxation peak to the orientation polarization of SnO_2 aggregated inside the ceramic whose traces appeared in XRD analysis as shown in **Figure 1**. From our previously published work for BTS and Er^{3+} doped BTS in the present work it is clearly observed that Er^{3+} substitute for Ti^{4+} caused the materials' grain growth process, besides promoting a change of the nature of the ferroelectricto-paraelectric phase transition from normal-like for BTSO to diffuse- and relaxor-like behavior. Moreover, when Er^{3+} substitute for Ba^{2+} does not show such effects [23], which confirms the substitution of Er^{3+} in Ti-site.

3.5.2. The Variation of the Permittivity (ε'), Dielectric Loss (ε''), Loss Tangent ($\tan\delta$) and ac Conductivity (σ_{ac}) as a Function of Frequency at Different Temperatures

The permittivity (ε') and the loss tangent ($\tan\delta$) of BTSO: 0.5Er and BTSO: 0.5Er1Yb ceramics as a function of frequency at different temperature (−50˚C, 0˚C, 50˚C, 100˚C and 150˚C) are shown in **Figure 6** and **Figure 7**. From **Figure 6**, it is seen that (ε') decreases with the increase in the frequency till 10^4 Hz for all temperature degrees. Beyond the frequency 10^4 Hz, (ε') becomes constant at all temperatures [41]. At low frequencies, the contribution from all polarization

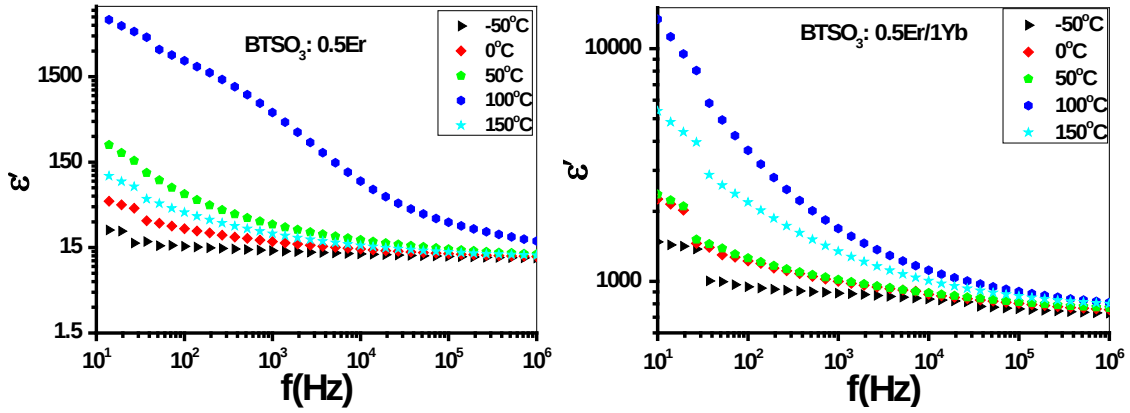

Figure 6. Variation of the permittivity (ε') of nano-structure BTSO: 0.5Er and BTSO: 0.5Er/1Yb ceramics as a function of frequency at different temperatures calcinated in the air for 4 hours at 1050˚C.

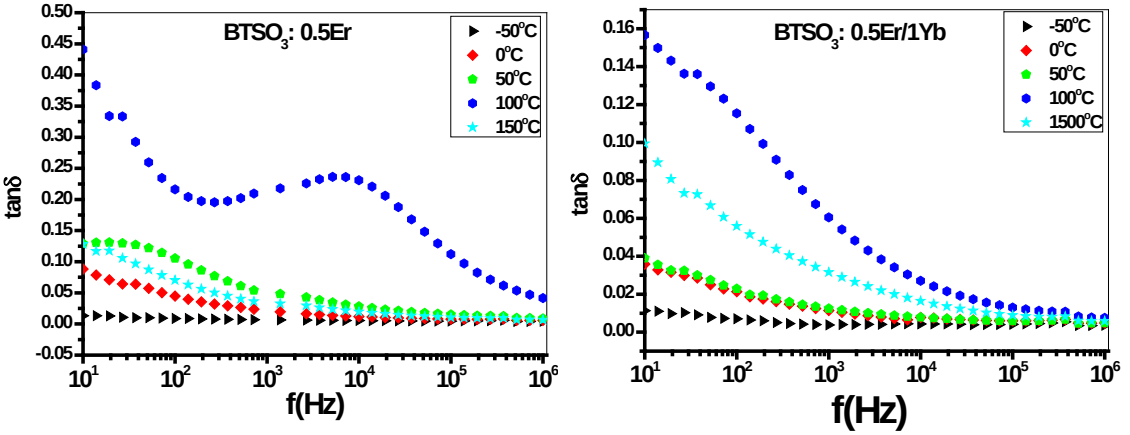

Figure 7. The frequency dependence of the dielectric loss tangent (tanδ) at different temperatures for BTSO: 0.5Er and BTSO: 0.5Er/1Yb calcinated in the air for 4 hours at 1050˚C.

components (dipolar, space charge, electronic and ionic polarization) is possible, giving rise to the increase in ε'values. Moreover, one can attribute this trend to the electrical field fast variation accompanying the frequency and the charge carrier scattering [42]. The obtained process leading to a dipole moment random orientation accordingly decreases the (ε') values. But as the frequency increases, one or more of the mentioned components will have no longer time to orient themselves towards the electric field, as a result of the total polarization decrease, then ε'decreases. This is a normal characteristic behavior for the dielectric materials [43].

Suddenly decrease in ε' is detected at above 100˚C up to 150˚C, leads to a phase transition occurred at Curie temperature (T_c) at 117 and 93˚C for both prepared samples; see **Figure 7**. At which the samples transformed to the paraelectric phase (un-polarized sate) from the ferroelectric phase (polarized state). Therefore the permanent dipole moment controlled polarization which in sequence affects the permittivity results from the displacement of the oxygen ions negatively charged and titanium ions positively charged from their balanced po-

sitions (increasing displacement). For that reason, a vertical direction elongation can be occurred bringing tetragonal phase. Then, the dielectric behavior of tetragonal BTSO: 0.5Er and BTSO: 0.5Er1Yb is in good agreement with that described by XRD, see **Figure 1**.

Instead, by heating the samples above, its own Curie temperature (T_c) and ε' are obviously decreased. This is because the formed tetragonal phase (non-symmetric) at lower temperature transformed into cubic phase (symmetric) at temperature higher than T_c [44].

While **Figure 7** shows that the nature of tanδ for all samples is the same as that for ε', (*i.e.*) tanδ at low frequency is high and steeply decreases with the frequency increase till certain frequency at 10^5 Hz, away from this frequency the tanδ gets nearly constant with the further increase in frequency of BTSO: 0.5Er and BTSO: 0.5Er1Yb.

Moreover, the (ε') decreased with the frequency increasing showing an abnormal dispersion. This mentioned dispersion in (ε') is together with a relaxation peak in tan δ as shown in **Figure 7**. This peak intensity is slightly increased and its maximum moved to lower frequencies by the increase in temperature for BTSO: 0.5Er and BTSO: 0.5Er/1Yb, respectively. Then it disappeared at lower temperature than 0˚C. The dispersive behavior of the (ε') is mainly due to two reasons: 1) associated mobile charge carriers and 2) the polarized structure of the studied material.

In addition to frequency and temperature dependency, the grain boundaries (GB), in homogeneity and domain walls have been considered as critical factors influencing the ceramic permittivity. As reported previously, the grain boundaries cause limiting the oxygen vacancies diffusion, particularly for nano fine -grained ceramics [37]. For the present ceramics, Ti^{3+} cations are considered as source of oxygen vacancies [45].

In nanocrystalline materials, majority of atoms exist in the grain boundary or in a few atomic layers from the boundary [46]. Oxide materials are reported to contain oxygen vacancies. The oxygen vacancy is equivalent to the positive charge and then possesses the dipole moment. In nano-structured material the defects density is very great. Accordingly, BTSO: 0.5Er and BTSO: 0.5Er1Yb grain boundaries should be rich in oxygen vacancies and thus should have high dipoles density [47] [48]. Open to an external electric field, the dipoles will rotate giving an increase in polarization of BTSO: 0.5Er and BTSO: 0.5Er1Yb. So the ε' high value in the regions of low and medium frequency can be explained for this type of polarization.

The σ_{ac} shows maximum values at 100˚C for the BTSO: 0.5Er and BTSO: 0.5Er-1Yb ceramics and increases by increasing the frequency, as shown in **Figure 8**, obeying Jonscher's universal power law ($\sigma_{ac} \alpha A\omega^s$) $\sigma_{ac} = \sigma_{dc} + A\omega^s$ [49]. On the other hand, σ_{ac} slightly increases by increasing the temperature, and then shows an anomaly near the transition or Curie temperature T_c. The conduction at low temperatures in the tetragonal structure (ferroelectric phase) is due to impurities or defects present in the sample such as oxygen vacancies which reported as the

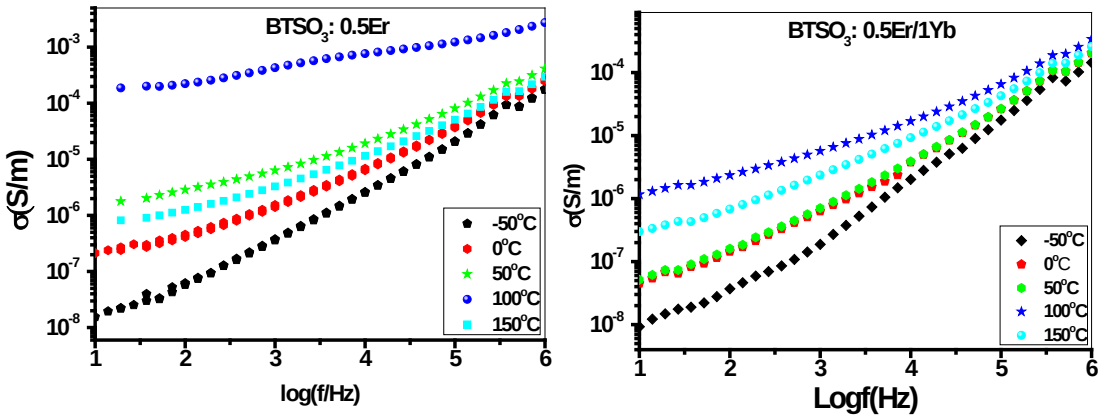

Figure 8. The frequency dependence of ac conductivity (σ_{ac}) at different temperatures for BTSO: 0.5Er and BTSO: 0.5Er/1Yb calcinated in the air for 4 hours at 1050˚C.

most mobile ionic defects in perovskite. At higher temperature ≥ T_c, the conduction is due to thermally activated ionic hopping of oxygen vacancies while the sample structure converted from tetragonal to cubic structure (paraelectric phase). For being Er^{3+} and Yb^{3+} ions acceptor dopants replacing titanium (Ti^{4+}) at the B-site perovskite lattice resulting in p-type conduction. Since Er^{3+} and Yb^{3+} ions have a different valence than Ti^{4+} ions, substitution by each produces a charge imbalance [50].

4. Conclusion

$BaTi_{0.9}Sn_{0.1}O_3$ doped with 0.5 mol% Er^{3+} ions and those co-doped with Er^{3+}/Yb^{3+} ions, were prepared using the modified sol-gel method. From the obtained results, it is possible to establish a relationship between the structure and the dielectric properties of doped and co-doped $BaTi_{0.9}Sn_{0.1}O_3$. The doped sample with Er^{3+} ions and those co-doped with Er^{3+}/Yb^3 ions affect the crystal structure by changing the tetragonality of the crystal lattice. It affected a change in phase transition temperature. The particle size was estimated using the Scherer equation and X-ray diffraction data. The significant grain size increases as a result of doping as agree with the XRD results. The values of crystallite size, lattice parameters, from XRD increases by increasing Yb^{3+} ions concentration. The crystallite size of BTSO: 0.5Er equal to 45.9 nm which increases to 47.20 then to 57.7 nm by increasing the co-doped concentration from 0.75 to 1 mol% of Yb, this may be because substitution of Ti^{4+} ions by Yb^{3+} ions having a larger radius. Characteristic bonding of BTSO: 0.5Er, BTSO: 0.5Er0.75Y bands BTSO: 0.5Er1Yb were observed with FTIR spectroscopy. FTIR results showed enhancement in crystallinity and absence of carbonates upon increasing Yb^{3+} ions concentration from 0.75 up to 1 mol%. TEM micrographs display that the particles have a nano-structure spherical shape with a small size. The average particle Size (P.S) from TEM of BTSO: 0.5Er is equal to 49.4 nm. These results are in agreement with the results obtained for crystallite sizes from the XRD study. FESEM micrographs of the surface and the grain sizes are observed in the range of 31 - 54

nm. The tetragonality decreased by increasing Yb^{3+} ions concentrations giving a more spherical shape and higher density. The observed changes in structure, morphology, and crystallite size of BTSO upon substituting by Er^{3+} and/or Er^{3+}/Yb^{3+} ions, result in changing the dielectric properties. The dielectric study of the BTSO: 0.5Er (A), BTSO: 0.5Er0.75Yb (B) BTSO: 0.5Er1Yb (C) calcinated at 1050˚C for 4 h in air permittivity (ε'), at different frequencies are studied for the first time. The permittivity behavior for samples confirmed the existence of a tetragonal phase for all samples, and a phase transition from a tetragonal to cubic phase at the Curie temperature. The Curie temperature (T_c) shifted to a lower value from 117 for BTSO: 0.5Er to 93 for BTSO: 0.5Er/1Yb and the permittivity ε' increased from 3972 to 6071, so BTSO: 0.5Er/1Yb good crystalline material candidate for capacitors application due to its higher permittivity. While the Er^{3+} substitute for Ti^{4+} caused the materials' grain growth process, besides promoting a change of the nature of the ferroelectric to paraelectric phase transition from normal-like for BTSO to diffuse- and relaxor-like behavior. Moreover, when Er^{3+} substitute for Ba^{2+} does not show such effects which previously reported, which confirms the substitution of Er^{3+} in Ti-site.

Conflicts of Interest

The authors declare no conflicts of interest regarding the publication of this paper.

References

[1] Xu, J., Menesklou, W. and Ivers-Tiffee, E. (2004) Processing and Properties of BST Thin Films for Tunable Microwave Devices. *Journal of the European Ceramic Society*, **24**, 1735-1739. https://doi.org/10.1016/S0955-2219(03)00485-0

[2] Lee, B.I. (1999) Chemical Variations in Barium Titanate Powders and Dispersants. *Journal of Electroceramics*, **3**, 53-63. https://doi.org/10.1023/A:1009966900092

[3] Zhu, X.N., Chen, X., Tian, H. and Chen, X.M. (2017) Atomic Scale Investigation of Enhanced Ferroelectricity in (Ba,Ca)TiO_3. *RSC Advances*, **7**, 22587-22591. https://doi.org/10.1039/C7RA00662D

[4] Rayssi, Ch., Kossi, S.El., Dhahri, J. and Khirouni, K. (2018) Frequency and Temperature-Dependence of Dielectric Permittivity and Electric Modulus Studies of the Solid Solution $Ca_{0.85}Er_{0.1}Ti_{1-x}Co_{4x/3}O_3$ ($0 \le x \le 0.1$). *RSC Advances*, **8**, 17139-17150. https://doi.org/10.1039/C8RA00794B

[5] Narang, S.B., Kaur, D. and Pubby, K. (2015) Frequency and Temperature Dependence of Dielectric and Electric Properties of $Ba_{2-x}Sm_{4+2x/3}Ti_8O_{24}$ with Structural Analysis. *Materials Science-Poland*, **33**, 268-277. https://doi.org/10.1515/msp-2015-0034

[6] Moya, X., Stern-Taulats, E., Crossley, S., González-Alonso, D., Kar-Narayan, S., Planes, A., Mañosa, L. and Mathur, N.D. (2013) Giant Electrocaloric Strength in Single-Crystal $BaTiO_3$. *Advanced Materials*, **25**, 1360-1365. https://doi.org/10.1002/adma.201203823

[7] Jain, A. and Panwar, A.K. (2020) Synergetic Effect of Rare-Earths Doping on the Microstructural and Electrical Properties of Sr and Ca Co-Doped $BaTiO_3$ Nanoparticles. *Ceramics International*, **46**, 10270-10278. https://doi.org/10.1016/j.ceramint.2020.01.020

[8] Kaddoussi, H., Gagou, Y., Lahmar, A., Allouche, B., Dellis, J.L., Courty, M., Khemakhem, H. and El Marssi, M. (2016) Ferroelectric Phase Changes and Electrocaloric Effects in $Ba(Zr_{0.1}Ti_{0.9})_{1-x}Sn_xO_3$ Ceramics Solid Solution. *Journal of Materials Science*, **51**, 3454-3462. https://doi.org/10.1007/s10853-015-9663-z

[9] Haddadou, N., Belhadi, J., Manoun, B., Taïbi, K., Carcan, B., El Marssi, M. and Lahmar, A. (2018) Structural, Vibrational, and Dielectric Investigations of $Ba_{0.925}Bi_{0.05}(Ti_{0.95-x}Zr_x)Sn_{0.05}O_3$ Ceramics. *Journal of Materials Science*: *Materials in Electronics*, **29**, 16144-16154. https://doi.org/10.1007/s10854-018-9703-y

[10] Marković, S., Mitrić, M., Jovalekić, C. and Miljković, M. (2007) Dielectric and Ferroelectric Properties of $BaTi_{1-x}Sn_xO_3$ Multilayered Ceramics. *Materials Science Forum*, **555**, 249-254. https://doi.org/10.4028/www.scientific.net/MSF.555.249

[11] Tsur, Y., Dunbar, T.D. and Randall, C.A. (2001) Crystal and Defect Chemistry of Rare Earth Cations in $BaTiO_3$. *Journal of Electroceramics*, **7**, 25-34. https://doi.org/10.1023/A:1012218826733

[12] Leyet, Y., Peña, R., Zulueta, Y., Guerrero, F., Anglada-Rivera, J., Romaguera, Y. and de la Cruz, J.P. (2012) Phase Transition and PTCR Effect in Erbium Doped BT Ceramics. *Journal of Materials Science and Engineering B*, **177**, 832-837. https://doi.org/10.1016/j.mseb.2012.03.048

[13] Zannen, M., Dietze, M., Khemakhem, H., Kabadou, A. and Es-Souni, M. (2014) The Erbium's Amphoteric Behavior Effects on Sodium Bismuth Titanate Properties. *Ceramics International*, **40**, 13461-13469. https://doi.org/10.1016/j.ceramint.2014.05.069

[14] Chalfouh, C., Lahmar, A., Zghal, S., Hannachi, R., Abdelmoula, N. and Khemakhem, H. (2017) Effects of Lanthanide Amphoteric Incorporation on Structural, Electrical, and Photoluminescence Properties of $BaTi_{0.925}(Yb_{0.5}Nb_{0.5})_{0.075}O_3$ Ceramic. *Journal of Alloys and Compounds*, **711**, 205-214. https://doi.org/10.1016/j.jallcom.2017.03.351

[15] Klugpand, P. and Alexander, L.E. (1954) X-Ray Diffraction Procedure. Wiley, New York, Chapter 9, 504-524.

[16] Zhang, K., Li, L., Wang, M. and Luo, W. (2020) Charge Compensation in Rare Earth Doped $BaTiO_3$-Based Ceramics Sintered in Reducing Atmosphere. *Ceramics International*, **46**, 25881-25887. https://doi.org/10.1016/j.ceramint.2020.07.072

[17] Khandelwal, A., Gupta, R., Laishram, R. and Singh, K.C. (2019) Impact of Crystal Structure and Microstructure on Electrical Properties of Ho Doped Lead-Free BCST Piezoceramics. *Ceramics International*, **45**, 10371-10379. https://doi.org/10.1016/j.ceramint.2019.02.095

[18] Ansari, M.A. and Sreenivas, K. (2019) Effects of Disorder Activated Scattering and Defect-Induced Phase on the Ferroelectric Properties of $BaSn_xTi_{1-x}O_3$ ($0 \le x \le 0.28$) Ceramics. *Ceramics International*, **45**, 20738-20749. https://doi.org/10.1016/j.ceramint.2019.07.058

[19] El-Sayed, O., Mousa, W.M., El-Mahy, S.K., Salem, M.A., Battisha, I.K., Mahani, R., Lahmer, A. and El Marssi, M. (2019) Photoluminescence, Structural, Morphology and Dielectric Properties of $BaTi_{0.9}Sn_{0.1}O_3$ Doped with Nd^{3+} and Nd^{3+}/Yb^{3+} Ions. *Journal of Scientific Research in Science*, **36**, 248-268. https://doi.org/10.21608/jsrs.2019.57630

[20] Ferrarelli, M.C., Tan, C.C. and Sinclair, D.C. (2011) Ferroelectric, Electrical, and Structural Properties of Dy and Sc Co-Doped $BaTiO_3$. *Journal of Materials Chemistry*, **21**, 6292-6299. https://doi.org/10.1039/c0jm04429f

[21] Dunbar, T.D., Warren, W.L., Tuttle, B.A., Randall, C.A. and Tsur, Y. (2004) Elec-

tron Paramagnetic Resonance Investigations of lanthanide-Doped Barium Titanate: Dopant Site Occupancy. *The Journal of Physical Chemistry B*, **108**, 908-917. https://doi.org/10.1021/jp036542v

[22] Zulueta, Y.A., Guerrero, F., Leyet, Y., Anglada-Rivera, J., Gonzalez-Romero, R.L. and Melendez, J.J. (2015) Can Erbium Dopant Occupy Both Cation Sites in Cubic Barium Titanate via a Mechanism Different than Self-Compensation? *Physica Status Solidi* (*b*), **252**, 508-516. https://doi.org/10.1002/pssb.201451034

[23] Harold, P. and Leroy, E. (1974) X-Ray Diffraction Procedure: For Polycrystalline and Amorphous Materials. Wiley, New York.

[24] Antonelli, E., Letonturier, M. and Mepeko, J.C. (2009) Microstructural, Structural and Dielectric Properties of Er^{3+}-Modified $BaTi_{0.85}Zr_{0.15}O_3$ Ceramics. *Journal of the European Ceramic Society*, **29**, 1449-1455. https://doi.org/10.1016/j.jeurceramsoc.2008.09.009

[25] Takada, K., Chang, E. and Smyth, D.M. (1987) Rare Earth Additions to $BaTiO_3$. *Advances in Ceramics*, **19**, 147-142.

[26] Takada, K., Ichimura, H. and Smyth, D.M. (1987) Equilibrium Conductivity for Er Doped $BaTiO_3$. *Japanese Journal of Applied Physics*, **26**, 42. https://doi.org/10.7567/JJAPS.26S2.42

[27] Thandar, W., Kyaw, N. and Khin, M.T. (2008) Synthesis of Barium Titanate from Titanyl Acylate Precursor by Sol-Precipitate Method. *Journal of the Myanmar Academy of Arts and Science*, **41**, 61-70.

[28] Gadkari, A.B., Shinde, T.J. and Vasambekar, P.N. (2009) Structural Analysis of Y^{3+}-Doped Mg-Cd Ferrites Prepared by Oxalate Co-Precipitation Method. *Materials Chemistry and Physics*, **114**, 505-510. https://doi.org/10.1016/j.matchemphys.2008.11.011

[29] Chavez, E., Fuentes, S., Zarate, R.A. and Padilla-Campos, L. (2010) Structural Analysis of Nanocrystalline $BaTiO_3$. *Journal of Molecular Structure*, **984**, 131-136. https://doi.org/10.1016/j.molstruc.2010.09.017

[30] Henderson, C.M.B., Charnock, J.M., Cressey, G. and Griffen, D.T. (1997) An EXAFS Study of the Local Structural Environments of Fe, Co, Zn and Mg in Natural and Synthetic Staurolites. *Mining Magazine*, **61**, 613-625. https://doi.org/10.1180/minmag.1997.061.408.01

[31] Wei, L.S., Lee, B.I. and Mann, L.A. (2000) Characterization of Carbonate on $BaTiO_3$ Ceramic Powders. *Materials Research Bulletin*, **35**, 1303-1312. https://doi.org/10.1016/S0025-5408(00)00331-7

[32] Carnall, W.T., Beitz, J.V., Crosswhite, H., Rajnak, K. and Mann, J.B. (1983) Spectroscopic Properties of the F-Elements in Compounds and Solutions. In: *Systematics and the Properties of the Lanthanides*, Springer, Dordrecht, 389-450. https://doi.org/10.1007/978-94-009-7175-2_9

[33] Mahani, R., El-Sayed, O., El-Mahy, S.K. and Battisha, I.K. (2020) Structure and Dielectric Studies of Sn^{4+}/Er^{3+} Co-Doped $BaTiO_3$ Nano-Powders. *Acta Physica Polonica A*, **137**, 410-416. https://doi.org/10.12693/APhysPolA.137.410

[34] Bucio, L., Orozcoand, E. and Tera, A.H. (2006) Relaxation and Conductivity Behaviour in the Compounds: $FeRGe_2O_7$ (R = Pr, Tb). *Journal of Physics and Chemistry of Solids*, **67**, 651-658. https://doi.org/10.1016/j.jpcs.2005.10.177

[35] Wei, X., Xu, G., Ren, Z., Wang, Y., Shen, G. and Han, G. (2008) Size-Controlled Synthesis of $BaTiO_3$ Nanocrystals via a Hydrothermal Route. *Materials Letters*, **62**, 3666-3669. https://doi.org/10.1016/j.matlet.2008.04.022

[36] Bitra, H.C.R. and Vara Prasad, B.B.V.S. (2014) Dielectric Studies of Nano Structured $BaTi_{1-x}Sn_xO_3$ Solid Solutions. *International Letters of Chemistry, Physics and Astronomy*, **13**, 191-201. https://doi.org/10.18052/www.scipress.com/ILCPA.32.191

[37] Garbarz-Glos, B., Lisińska-Czekaj, A., Czekaj, D. and Bąk, W. (2016) Effect of Semiconductor Element Substitution on the Electric Properties of Barium Titanate Ceramics. *Archives of Metallurgy and Materials*, **61**, 887-890. https://doi.org/10.1515/amm-2016-0150

[38] Upadhyay, S.K., Reddy, V.R., Bag, P., Rawat, R., Gupta, S.M. and Gupta, A. (2014) Electro-Caloric Effect in Lead-Free Sn Doped $BaTiO_3$ Ceramics at Room Temperature and Low Applied Fields. *Applied Physics Letters*, **105**, Article ID: 112907. https://doi.org/10.1063/1.4896044

[39] Suyver, J.F., Grimm, J., Van Veen, M.K., Biner, D., Krämer, K.W. and Güdel, H.U. (2006) Upconversion Spectroscopy and Properties of $NaYF^4$ Doped with Er^{3+}, Tm^{3+} and/or Yb^{3+}. *Journal of Luminescence*, **117**, 1-12.

[40] Zhao, H., Zhou, R. and Boa, H. (2020) Effect of La_2O_3 Doping on Dielectric Properties of $BaZr_{0.1}Ti_{0.9}O_3$ Ceramics by SOL-GEL Method. *Digest Journal of Nanomaterials and Biostructures*, **15**, 311-317.

[41] Gajula, G.R., Kumar, K.C., Buddiga, L.R. and Vattikunta, N. (2019) High Frequency Studies on Dielectric, Impedance and Nyquist Properties of $BaTiO_3$-$Li_{0.5}Fe_{2.5}O_4$ Composite Ceramics Substituted with Sm and Nb for Microwave Device Applications. *Journal of Materials Science*: *Materials in Electronics*, **30**, 3889-3898. https://doi.org/10.1007/s10854-019-00674-w

[42] Xu, N., Pu, Y.P., Wang, B., Wu, H.D. and Chen, K. (2012) Microstructure and Electrical Properties of $BaTiO_3$/Cu Ceramic Composite Sintered in Nitrogen Atmosphere. *Ceramics International*, **38**, S249-S53. https://doi.org/10.1016/j.ceramint.2011.04.094

[43] Behera, B., Nayak, P. and Choudhary, R.N. (2007) Dielectric Anomaly in $LiCa_2V_5O_{15}$ Ceramics. *Materials Letters*, **61**, 3859-3862. https://doi.org/10.1016/j.matlet.2006.12.048

[44] Willander, M., Nur, O., Israr, M., Hamad, A., El Desouky, F., Salem, M.. and Battisha, I. (2012) Determination of A.C. Conductivity of Nano-Composite Perovskite $Ba_{(1-x-y)}Sr_{(x)}TiFe_{(y)}O_3$ Prepared by the Sol-Gel Technique. *Journal of Crystallization Process and Technology*, **2**, 1-11. https://doi.org/10.4236/jcpt.2012.21001

[45] Nur, O., Willander, M., Israr, M.Q., Desouky, F., Salem, M.A., Abou Hamad, A.B. and Battisha, I.K. (2012) Effect of Elevated Concentrations of Strontium and Iron on the Structural and Dielectric Characteristics of $Ba_{(1-x-y)}Sr_{(x)}Ti\ Fe_{(y)}O_3$ Prepared through Sol-Gel Technique. *Journal of Physics B*, **407**, 2697-2704. https://doi.org/10.1016/j.physb.2012.03.023

[46] Battisha, I.K., Abou hamad, A.B. and Mahani, R. (2009) Structure and Dielectric Studies of Nano-Composite Fe_2O_3: $BaTiO_3$ Prepared by Sol-Gel Method. *Physica B*: *Condensed Matter*, **404**, 2274-2279. https://doi.org/10.1016/j.physb.2009.04.038

[47] Devi, S. and Jha, A.K. (2009) Structural, Dielectric and Ferroelectric Properties of Tungsten Substituted Barium Titanate Ceramics. *Asian Journal of Chemistry*, **21**, 117-124.

[48] AsifIqbal, M., Islama, M.U., Ali, I., Azhar khan, M. and Sadiq, I. (2014) High Frequency Dielectric Properties of Eu^{+3}-Substituted Li-Mg Ferrites Synthesized by Sol-Gel Auto-Combustion Method. *Journal of Alloys and Compounds*, **586**, 404-410. https://doi.org/10.1016/j.jallcom.2013.10.066

[49] Jonscher, A.K. (1977) The "Universal" Dielectric Response. *Nature*, **267**, 673-679. https://doi.org/10.1038/267673a0

[50] Ravel, B., Stern, E.A., Vedrinskii, R.I. and Kraizman, V. (1998) Local Structure and the Phase Transitions of $BaTiO_3$. *Ferroelectrics*, **206**, 407-430. https://doi.org/10.1080/00150199808009173